Advanced Time Series Analysis: Computer Exercise 3

Autumn 21, 01622
Assignment 3
December 10, 2021

Magne Egede Rasmussen, s183963,
Nicolaj Hans Nielsen, s184335
& Anton Ruby Larsen, s174356

Danmarks
Tekniske Universitet

Contents

1 Part 1

We are to simulate the Bonhoeffer-Van der Pol system which is given by

$$\begin{aligned} \frac{dx_1}{dt} &= \theta_3 \left(x_1 + x_2 - \frac{1}{3}x_1^3 + \theta_4 \right) \\ \frac{dx_2}{dt} &= -\frac{1}{\theta_3} \left(x_1 + \theta_2 x_2 - \theta_1 \right) \end{aligned} \tag{1.1}$$

The parameters are given to be

$$(\theta_1, \theta_2, \theta_3, \theta_4) = (0.7, 0.8, 3.0, -0.34)$$

which gives a limit cycle. The system should describe the firing of a single neuron but because nature is stochastic we incorporate some noise in 1.1 giving the new system.

$$\begin{aligned} \frac{dx_1}{dt} &= \theta_3 \left(x_1 + x_2 - \frac{1}{3}x_1^3 + \theta_4 \right) \mathrm{d}t + \sigma \mathrm{d}W_t \\ \frac{dx_2}{dt} &= -\frac{1}{\theta_3} \left(x_1 + \theta_2 x_2 - \theta_1 \right) \mathrm{d}t \end{aligned} \tag{1.2}$$

Where $\mathrm{d}W_t$ is a standard Wiener-process and σ is the incremental standard deviation of the noise. In order to simulate 1.2 we will use the Euler-Maruyama scheme but in order to use this scheme we need to discretize the system. The discretized system is given by

$$\begin{aligned} Y_{n+1}^1 &= Y_n^1 + \theta_3 \left(Y_n^1 + Y_n^2 - \frac{1}{3}\left(Y_n^1\right)^3 + \theta_4 \right) \Delta + \sigma \Delta W_{n+1}^1 \\ Y_{n+1}^2 &= Y_n^2 - \frac{1}{\theta_3} \left(Y_n^1 + \theta_2 Y_n^2 - \theta_1 \right) \Delta \end{aligned} \tag{1.3}$$

We will simulate 1.3 with $\Delta = 2^{-9}$, $\sigma = (0.0, 0.1, 0.2, 0.3, 0.4)$, $T \in [0, 100]$ and initial conditions $Y_0 = [-1.9, 1.2]$.

We first simulate with $\sigma = 0.0$ which is actually a discretization of the non-stochastic system 1.1.

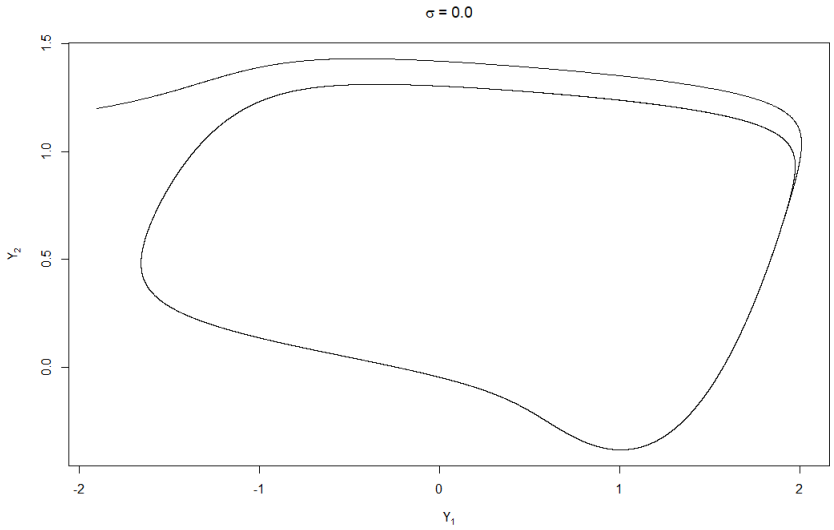

Figure 1

From figure 1 that when $\sigma = 0.0$ the system results in a limit cycle. We now add noise to the system.

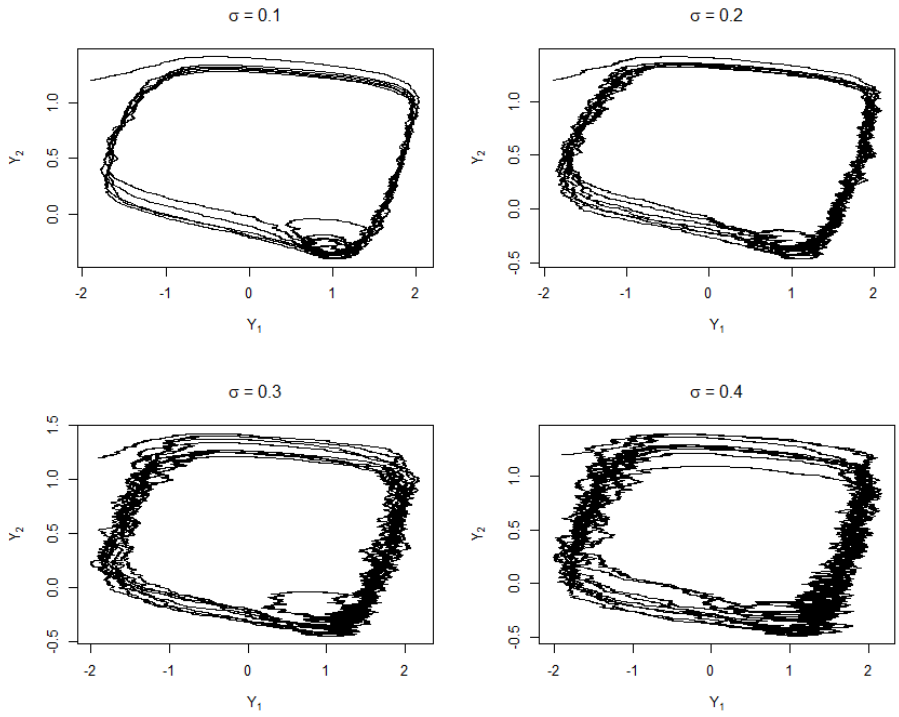

Figure 2

We now observe that we still have the orbiting behaviour as in the deterministic system but new behaviour has appeared in the bottom part of the cycle. We see especially in the $\sigma = 0.1$ case, a concentration of smaller cycles in the lower right of the large cycle and a separation of the orbits in the lower part of the large cycle. As the noise get larger this new behaviour gets harder and harder to distinguish from the noise. To investigate this further we expand the plots with a temporal dimension.

We again start with the deterministic case but before commenting on both the deterministic and stochastic case, we should point out that the base level in the histograms are changed from 0 to -100 to be able to distinguish little activity from no activity.

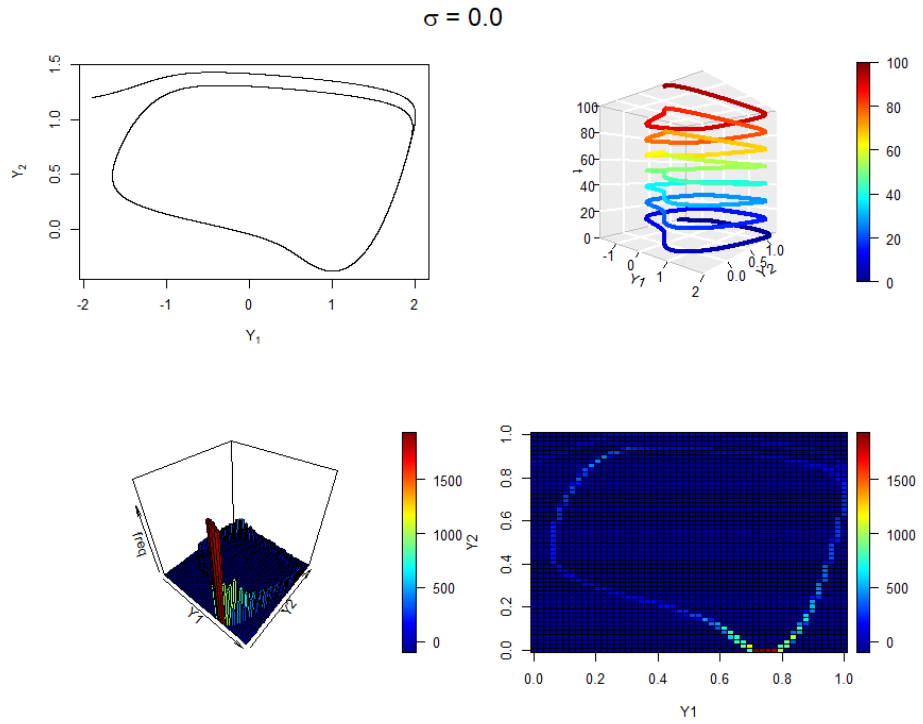

Figure 3

In the top right of figure 3 we see regular curves moving on the same spatial limit cycle through time as expected for the deterministic system. What is much more interesting is the two histograms in the bottom of figure 3. Here we see that much more time is spend in the bottom of the limit cycle. This is called bifurcation memory or a ghost in Strogatz literature. This indicates the system is near a bifurcation which we will see in the remaining.

Next we include noise and look at $\sigma = 0.1$, $\sigma = 0.2$, $\sigma = 0.3$ and $\sigma = 0.4$ in respectively figure 4, 5, 6 and 7.

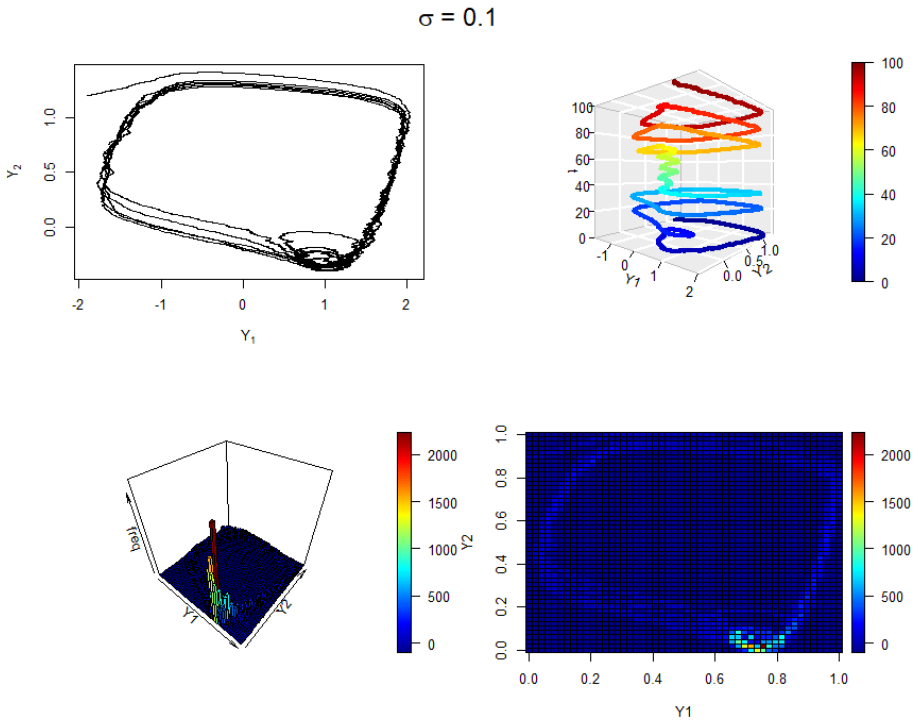

Figure 4

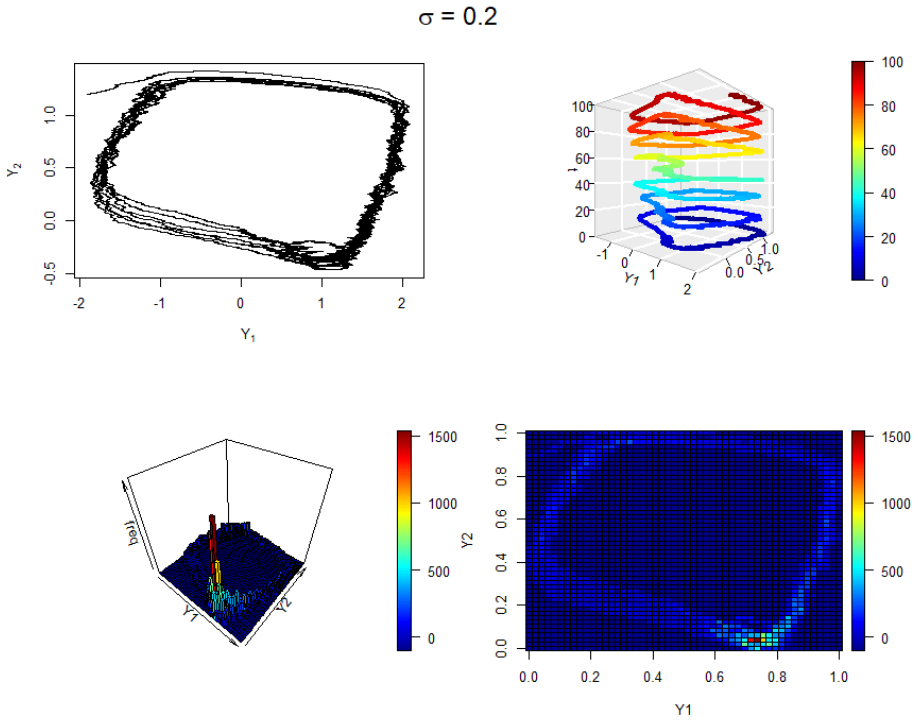

Figure 5

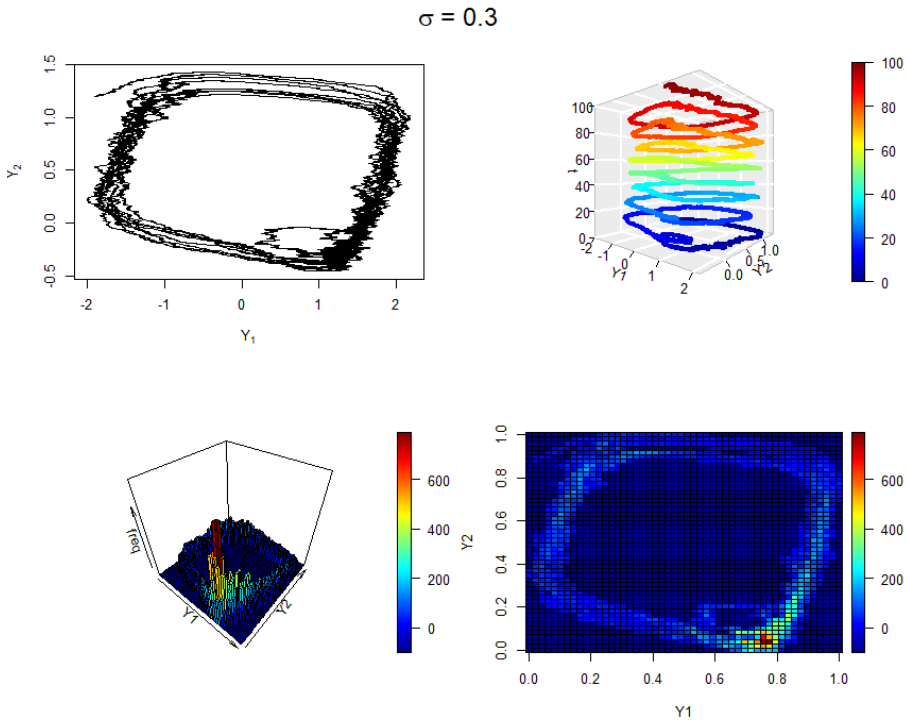

Figure 6

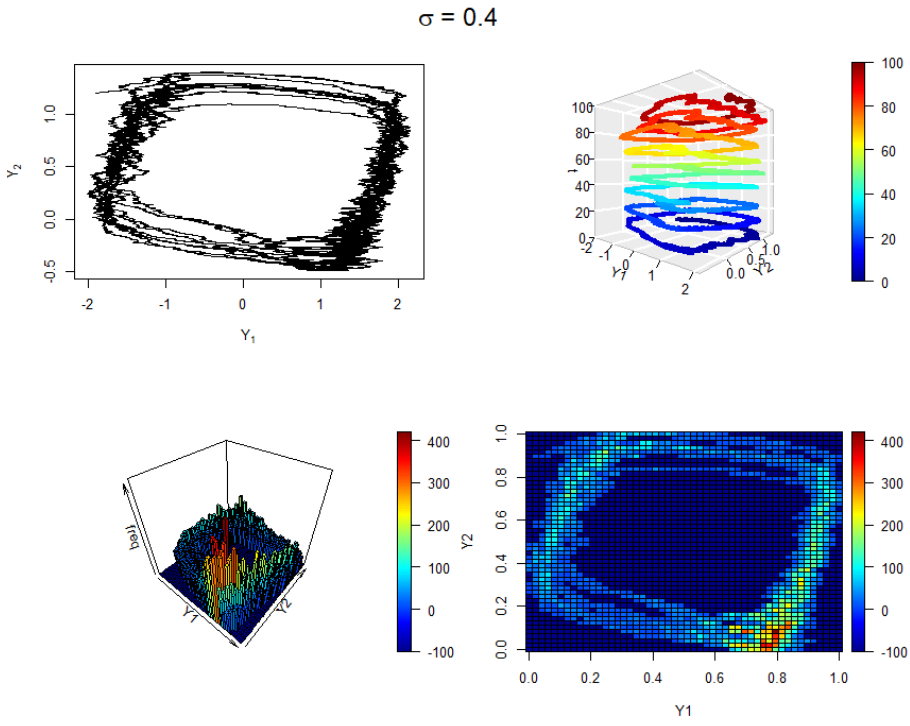

Figure 7

Especially in the $\sigma = 0.1$ case illustrated in figure 4, we see that between time 40 and 60 the large limit cycle collapse into a stable node. This behaviour can also be seen in the $\sigma = 0.2$ and $\sigma = 0.3$ case bot to lesser extent. In the $\sigma = 0.4$ case the noise level is so large that this dynamic disappears.

1.1 Hopf bifurcation

We will now investigate the bifurcation we discovered in the previous section. To do this we will substitute the Wiener process in 1.3 with a deterministic parameter c.

$$\begin{aligned} Y_{n+1}^1 &= Y_n^1 + \left(\theta_3 \left(Y_n^1 + Y_n^2 - \frac{1}{3}\left(Y_n^1\right)^3 + \theta_4\right) + c\right)\Delta \\ Y_{n+1}^2 &= Y_n^2 - \frac{1}{\theta_3}\left(Y_n^1 + \theta_2 Y_n^2 - \theta_1\right)\Delta \end{aligned} \tag{1.4}$$

We now vary the parameter c and simulate the system.

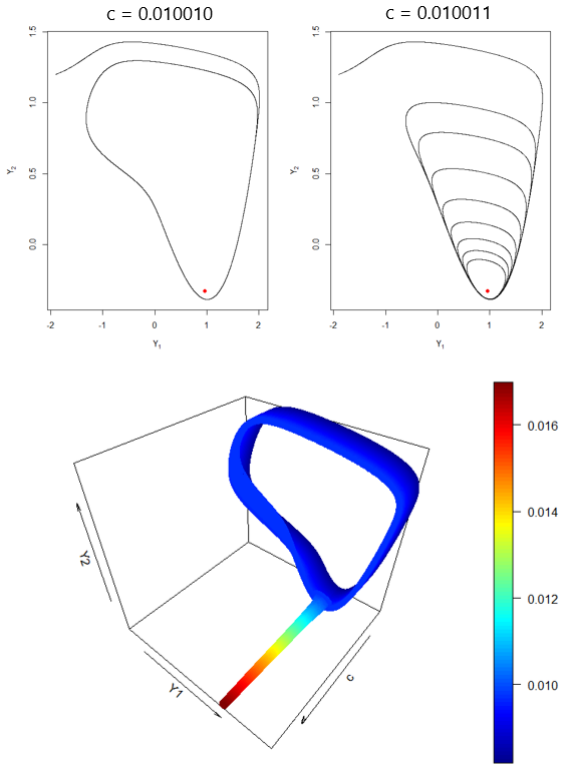

Figure 8

We see in figure 8 that when $c \gtrapprox 0.010011$ the limit cycle collapse into a stable node. This kind of bifurcation is called a supercritial Hopf bifurcation and the bifurcation diagram for the system is shown in the bottom of figure 8. We saw in figure 4-7 that for low levels of noise we could get "trapped" in the stable node but for larger levels of noise the bifurcation was not visible. The reason why we can get "trapped" for low-noise levels is that the c-value which it requires to return back to the limit cycle is higher than $c \gtrapprox 0.010011$. For high-noise system though the noise produced is so large that we can jump back and forth without problems and hence we do not see this "trapping".

1.2 Stationary Distribution

In the results above, we have presented the given stochastic differential equation based on simulations performed using the classic Euler-Marayama approximation. Running long time simulations we have also found approximate heat maps of the system behavior for different values of the diffusion scaling σ.

In this section we extend these results by calculations of stationary distributions. In other words, we extract the heat map of the system for $t \to \infty$. To perform an analysis of stationary distribution we discretizes our advection-diffusion equations into a two dimensional grid using finite-volume methods. We handle boundary conditions of our grid by reflection.

1.2.1 Theory on Stationary distributions

Stationary distributions are considered as important for stochastic differential equations as equilibrium points for ordinary differential equations [1]. To understand how to find stationary distributions, we briefly introduce the forward Kolmogorov equation. The equation governs the transition probabilities $\phi(t, y) = p(s \to t, x \to y)$, where the endpoint at t is y and the initial condition $X_s = x$. Under the assumption that X_t admits a probability density for $t > s$, the forward Kolmogorow equation is given by

$$\dot{\phi} = -\nabla \cdot (f\phi) + \nabla \cdot \nabla(D\phi) \tag{1.5}$$

for all $t \geq s$ and for all $y \in \mathbb{R}^n$. Here the diffusivity, D matrix is

$$D(y, t) = \frac{1}{2} g(y, t) g^{\top}(y, t) \tag{1.6}$$

Introducing the advective field

$$u = f - \nabla D \text{ where } (\nabla D)_i = \sum_j \frac{\partial D_{ij}}{\partial x_j} \tag{1.7}$$

we can now write eq. (1.5) in the form:

$$\dot{\phi} = -\nabla \cdot (u\phi - D\nabla\phi) \tag{1.8}$$

The two forms eq. (1.5) and eq. (1.8) are equivalent. The advection-diffusion equation eq. (1.8) is often prefered, as it expresses how probability is redistributed in space. Hence, it is also known as the conservative form. In operator form eq. (1.5) is written $\dot{\phi} = L^*\phi$.

In situations, when neither the drift nor the diffusion terms from the stochastic differential equations depend on time, the forward Kolmogorov equation often admits a stationary density denoted $\pi(x)$. Specifically to be a stationary distribution, $\pi(x)$ must satisfy:

$$L^*\pi = -\nabla \cdot (u\pi - D\nabla\pi) = 0 \tag{1.9}$$

Note that eq. (1.9) indeed tells that no probability is redistributed in our space. Hence if the initial condition X_s is sampled from the stationary distribution, then X_t will also follow the stationary distribution for every $t > s$. Thus the Markov property assures that all process statistics are independent of time. In general, stochastic differential equations may have many stationary distribution, a single unique or none. If there is a unique stationary distribution, the distribution X_t converges the same distribution no matter how we choose our initial condition X_s, when $t > s$ converges to infinity.

1.2.2 Numerical analysis

It is a common choice to discrete linear partial differential equations (like Kolmogorov equations) when computing the transition probability densities in small dimension. For the forward Kolmogorov equation this simply means:

$$\dot{\phi} = L^* \phi \mapsto \dot{\bar{\phi}} = \bar{\phi} G \tag{1.10}$$

where G is generator matrix. The method is also called 'the method of lines'.

The r function fvade2D from SDETools [2] is build upon the theory above. Its method to find the generator matrix includes the use of Euler-Marayama approximations. Hence, there can be some numerical errors when determining the stationary distribution (just as there might be some numerical errors for the simulations in the first part). For high values of σ the numerical difference vanishes with respect to the amount of added noise.

We find the following stationary distributions for the system described in eq. (1.3):

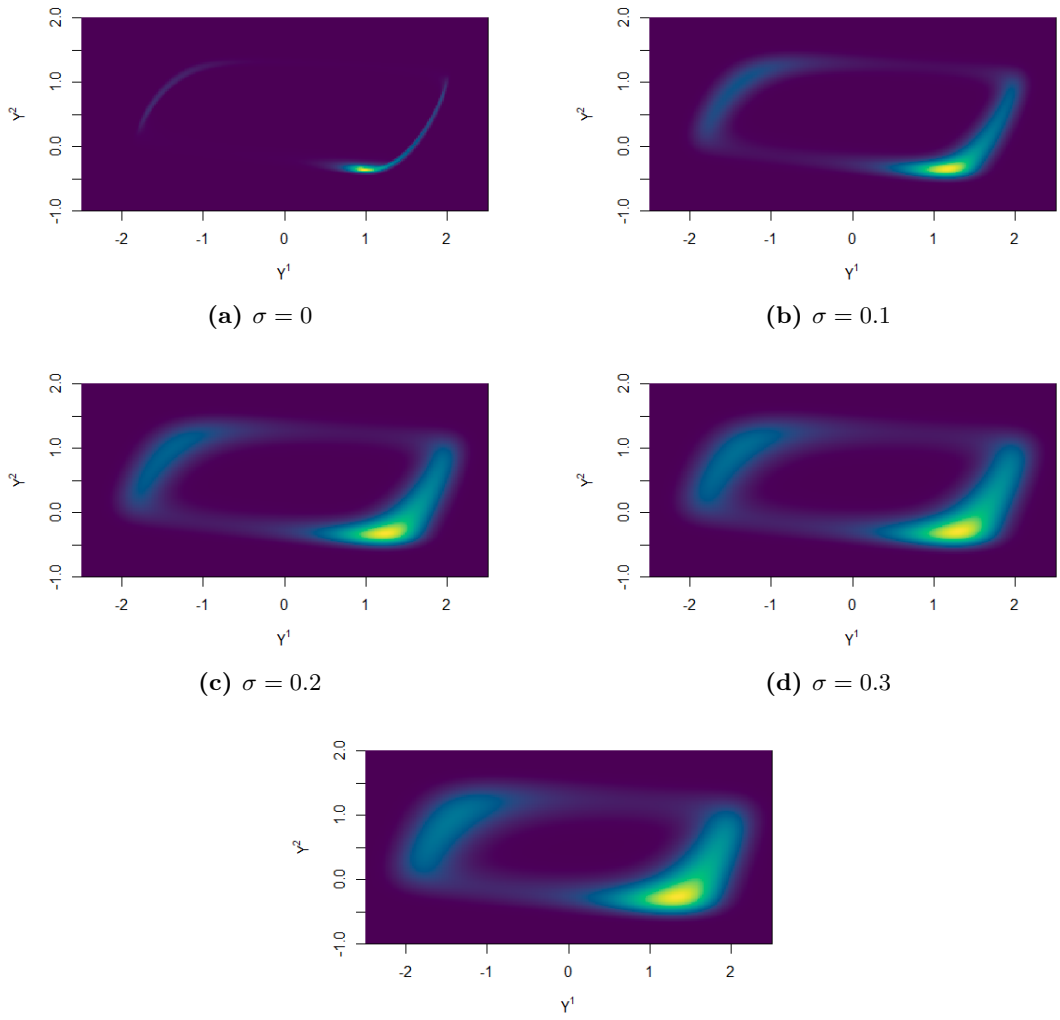

(a) $\sigma = 0$ **(b)** $\sigma = 0.1$

(c) $\sigma = 0.2$ **(d)** $\sigma = 0.3$

(e) $\sigma = 0.4$

Figure 9 – Stationary Distributions using fvade2D. The illustrations align with simulations shown in figure 4, 5, 6 and 7 for all values of the diffusion scale σ.

2 Part 2

In part 2 of Computer Exercise 3 we are set to model a building belonging to the University of Basque Country. In short, the building consists of 3 wings each having 4 floors. For simplicity we only look at the second floor of the east most wing. Fig. 10 gives an inside of the floor interior and available measures.

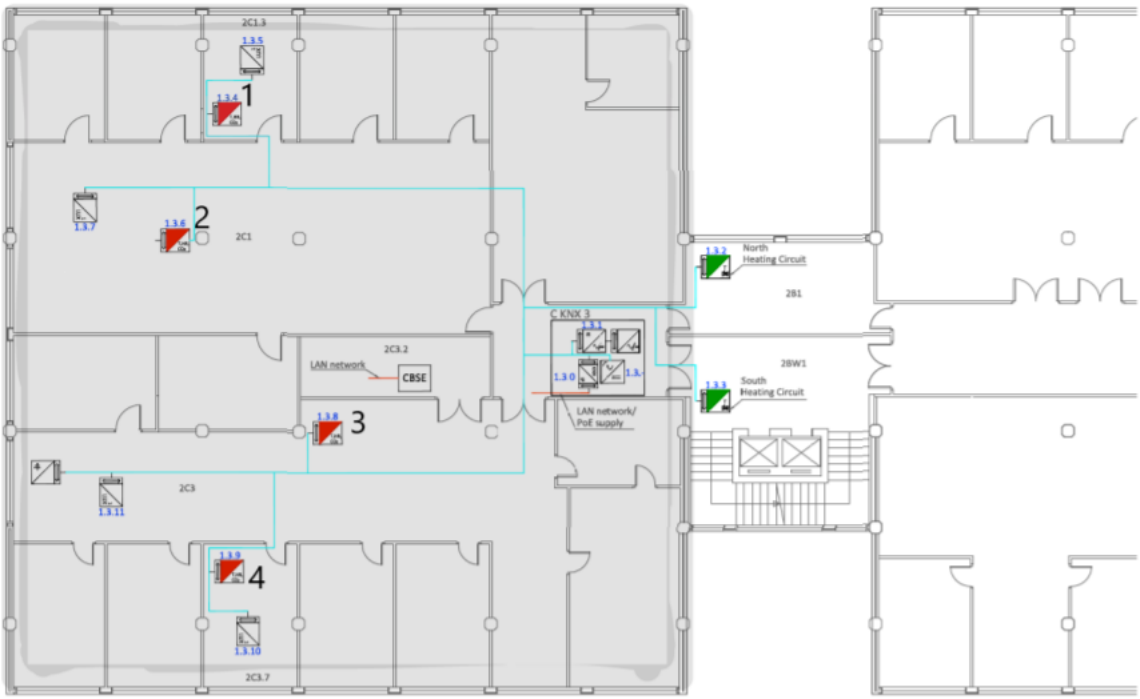

Figure 10 – North facing floor plan of the second floor of the east-most wing.

The four red devices on the floor plan are temperature sensors, while the blue routes denote heating circuits of radiators. Hence the heating close to sensor 1 and 2 can not be distinguished. The same accounts for temperature sensor 3 and 4.

Having looked into the floor plan of the building we aim to model, we look at our available data. Data is sampled hourly and provided in the period 22/12 - 2014 to 30/04 - 2015. In table 1 a small snippet is shown:

Name	Description	Unit	Index 40	Index 41	Index 42
date	Date and time	YY-MM-DD hh	14-12-24 00	14-12-24 01	14-12-24 02
t	Time since start	Hour	1272	1273	1274
$yTi1$	Temperature 1	$C°$	22.6	22.4	22.2
$yTi2$	Temperature 2	$C°$	22.8	22.7	22.6
$yTi3$	Temperature 3	$C°$	22.7	22.7	22.6
$yTi4$	Temperature 4	$C°$	22.7	22.6	22.5
Ta	Ambient temperature	$C°$	5.0	4.4	3.8
Gv	Global horizon solar radiation	W/m^2	0	0	0
$Ph1$	Heating in northern circuit	W	0.96	1.33	1.67
$Ph2$	Heating in southern circuit	W	2.75	2.69	3.44

Table 1 – Description of data available for modelling the building. Additionally, index 40, 41 & 42 has been included to illustrate the structure of the data set.

2.1 Data Exploration

In fig. 11 we look at the relationship between our given inputs. In the brief notes below we try to extract the main correlations results:

Room temperatures All four rooms are strongly linearly correlated. Hence, their internal relation is of use when modelling. We also see a positive correlation both with respect to time and ambient temperature.

Ambient temperature The correlation between the ambient temperature and the solar radiation Gv is not strong, however, there seems to be a clear linear trend when $Gv \neq 0$. This makes sense as the temperature increases when the sun is up, and is 0 during the nights.

Heating circuits The two separated heating systems are internally highly correlated which aligns with the room temperatures been highly correlated. Further, we see a clear negative correlation with ambient temperature as expected.

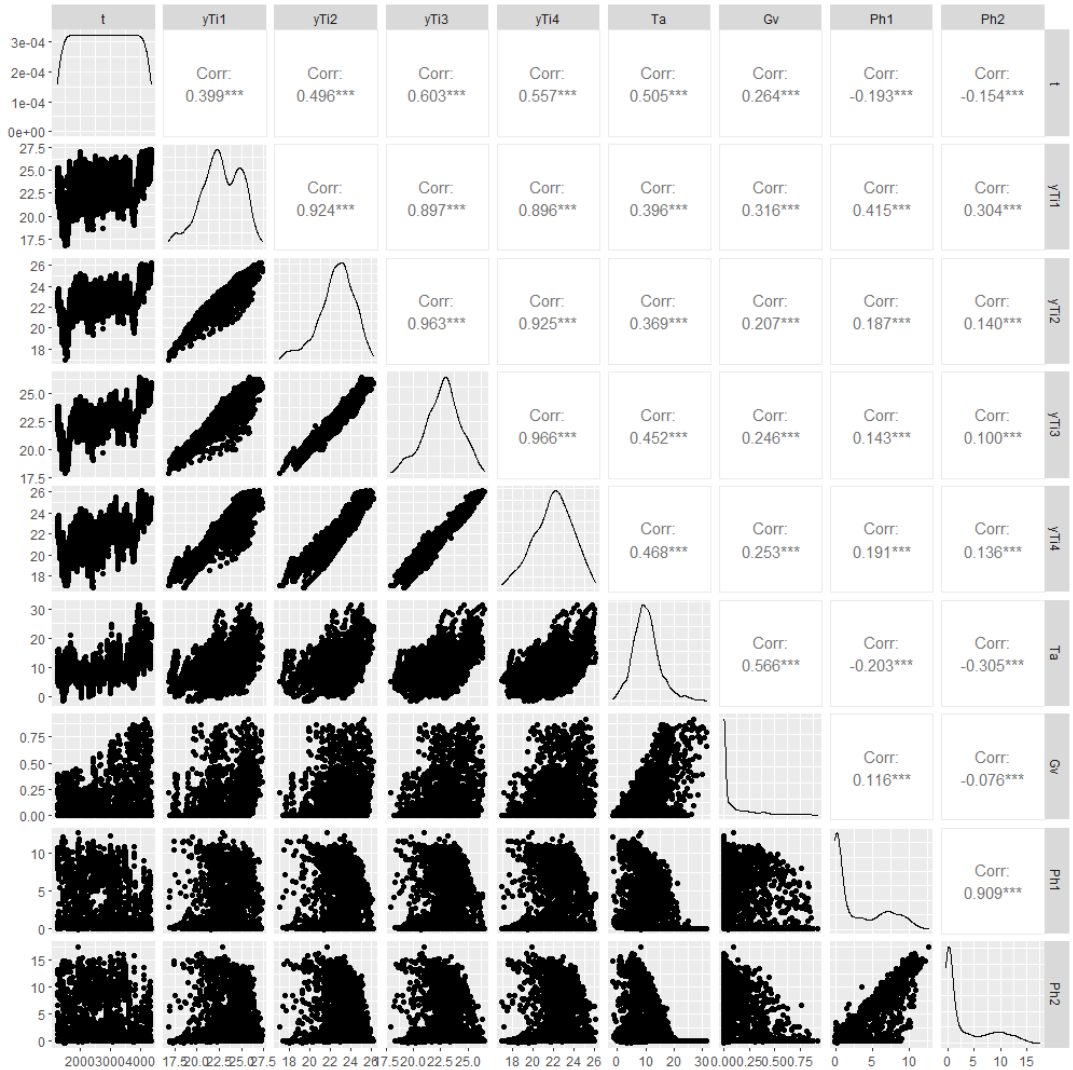

Figure 11 – Correlations in the given input data.

2.1.1 Visually inspection

To get an overall idea about the type of data, we work with, we consider the available data seres for room 1.

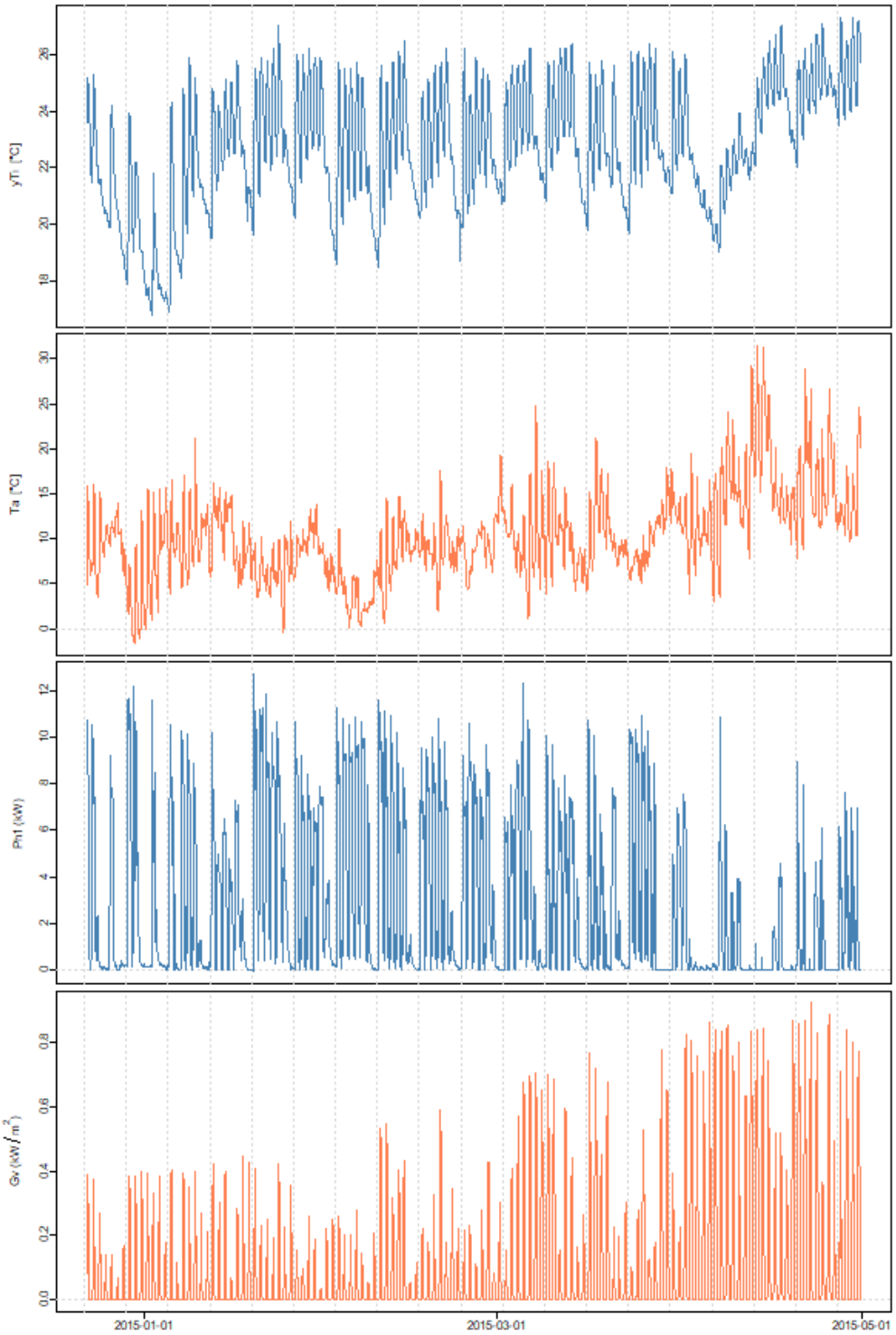

Figure 12 – All series initially considered for room 1. The vertical lines marks the beginning of a new week.

In fig. 12 we see the following patterns. The comments will not try to propose any reasons for the patterns observed.

1. yTi initially seems to have a negative trend. Then it goes into a more regular pattern for a long period until it hits some irregularity in one week.
2. the ambient temperature, Ta, has some irregular patterns for a long time though in the end of the series, there seems to be a general shift towards higher values.
3. the heating device Ph1 is initially not turned on as much. Ph1 starts to increase when yTi is also increasing a bit later and then it follows a regular pattern for some time. A bit later when Ta increases, it seems that Ph1 decreases.
4. The solar radiation Gv is initially quite low, however, it increases towards the end of the period especially when Ta is also increasing

We have to predict the indoor room temperature and to get an idea of the daily and weekly fluctuations during a normal business week, we have zoomed in on three normal business weeks in January for room 1, yTi1:

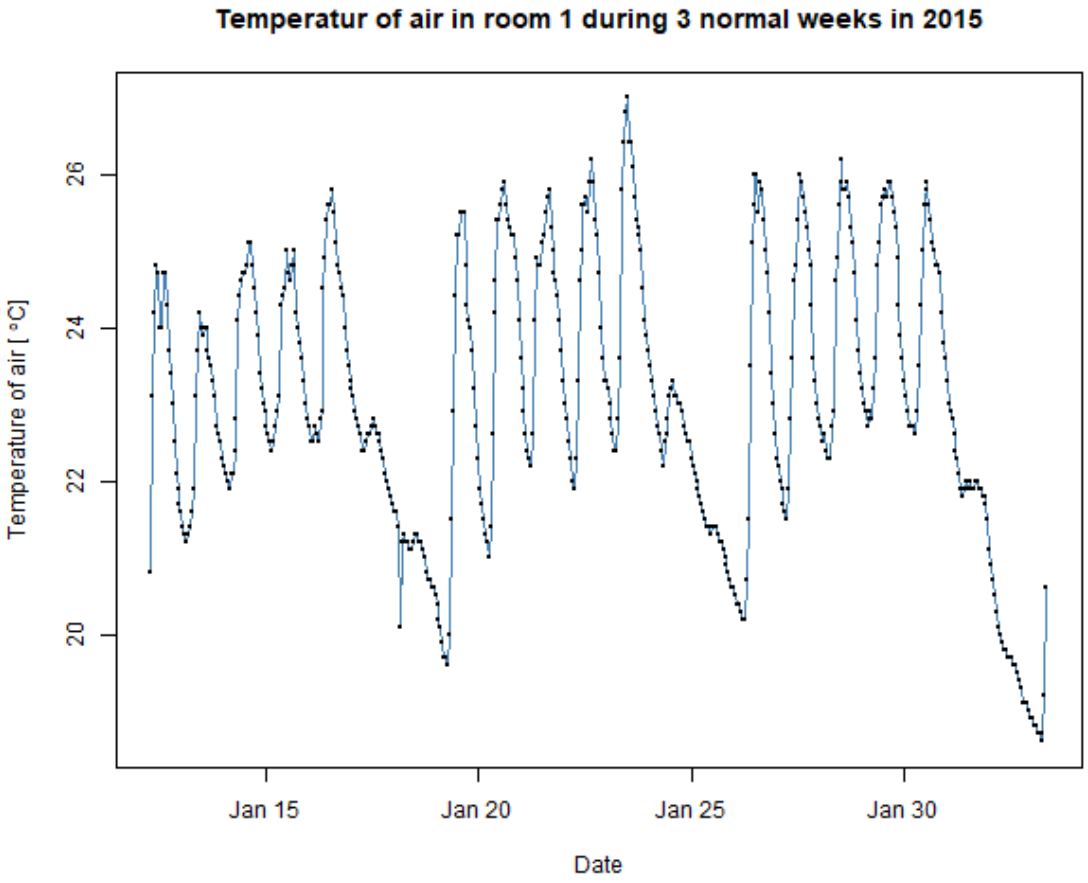

Figure 13 – 3 usual business weeks in January for room 1, yTi1.

Fig. 13 reveals the following patterns:

1. in the weekends, the temperature is much lower than during a usual weekday. Further, there seem to be a difference between Saturday and Sunday.
2. there are peak hours during the day where the temperature is higher.
3. it seems that the inertia in the building forces a positive linear trend through a work week. The trend can also be seen looking at the minimum temperature each day. Here the growth through the weekdays looks logistic.
4. we see a couple of outliers.

The data exploration has shown that multiple variables and trends seem to affect indoor temperatures. Having extracted some of the main influences, we decide to improve the complexity by adding them to the models step by step. The processes are explained through respectively section 2.2 where more and more significant variables will be included.

2.2 Part 2a & 2b: Modelling a Single Room

Through Part 2a and 2b we aim to model the indoor temperature in a single room, specifically we have chosen to model the room with temperate sensor 1. The room is fairly small and positioned at the exterior. Hence we assume the room to be highly influence by global weather behavior.

2.2.1 Baseline Model

In the task description, we are provided with stochastic differential equations as our baseline model. Choosing to model room temperatures dynamically, we can sufficiently apply the Markov property of continuous processes. Hence the next step is given only based on the current. Model wise, the baseline model can therefore be written as:

$$\begin{aligned} dT_i &= \frac{1}{C_i}\left(\frac{1}{R_{ia}}(T_a - T_i) + \frac{1}{R_{im}}(T_m - T_i) + \Phi + A_w G_v\right)dt + \sigma_1 dw_1 \\ dT_m &= \frac{1}{C_m}\left(\frac{1}{R_{im}}(T_i - T_m)\right)dt + \sigma_2 dw_2 \\ yT_i &= T_i + \varepsilon \end{aligned} \tag{2.1}$$

In eq. (2.1) T_i and T_m are the temperatures of the air and thermal mass of the room respectively. We use T_i to predict yT_i which is the indoor temperature we have observed. Further, C_i and C_m denotes the corresponding heat capacities, while R_{im} is the thermal resistance between the two. R_{ia} is similarly given as the thermal resistance from the internal air and the outside.

Comparing our estimated yT_i based on eq. (2.1) with the actual indoor temperature in room 1, the baseline results output:

RSS	BIC
404.90	2485.9

Table 2 – Baseline results

To know what these error metrics and information criteria means for the errors of the model, we will visually inspect them:

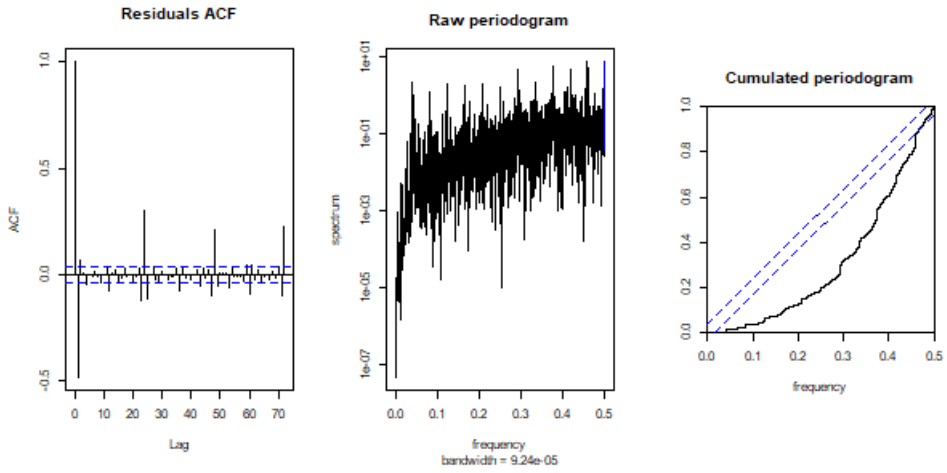

Figure 14 – Residual analysis for the baseline model of eq. (2.1)

In fig. 14, we see the residuals are far from white and there is a great deal of systematic variation that the baseline model cannot describe. The errors also varies over the day as seen in fig. 15 where we see a larger deviation from 9-19 a.m. With this analysis, we now know what the metrics of table 2 amounts to in terms actual errors and to shorten the analysis we will only provide RSS and BIC and focus on reducing errors for specific hours and hence display the distribution of errors across the 24 hours of the day fig. 15.

2.2.2 Exploiting Thermal Mass

The differential equation for T_m in the baseline model is very simple. Its drift term is only dependent on the difference between the indoor air temperature and thermal mass. Hence, to improve the modelling of T_m and thereby indirectly yT_i we add two new influences to the thermal mass: p is constrained between 0 and 1. Thus, it aims to distinguish between solar radiation impacting air temperature and solar radiation impacting thermal mass. Finally, we also add an impact from the ambient temperature on the thermal mass. Room 1 is an exterior room and therefore we assume a direct influence of the outside temperature on the thermal mass as well.

$$\begin{aligned} dT_i &= \frac{1}{C_i}\left(\frac{1}{R_{ia}}(T_a - T_i) + \frac{1}{R_{im}}(T_m - T_i) + \Phi + A_w G_v p\right) dt + \sigma_1 dw_1 \\ dT_m &= \frac{1}{C_m}\left(\frac{1}{R_{im}}(T_i - T_m) + \frac{1}{R_{ma}}(T_m - T_a) + A_w G_v (1-p)\right) dt + \sigma_2 dw_2 \\ yT_i &= T_i + \varepsilon \end{aligned} \tag{2.2}$$

The new parameters optimized by CTSM are $p = 0.47$ and $R_{ma} = 21.9$ and both significant. Adding significant terms to our dynamic model we expect a higher accuracy, which indeed is highlighted in table 3.

RSS	BIC
323.47	1796.3

Table 3 – Thermal mass complexity results

The residual sum of squares remains very high. To identify where we can perform significantly better, we plot our residuals through a day:

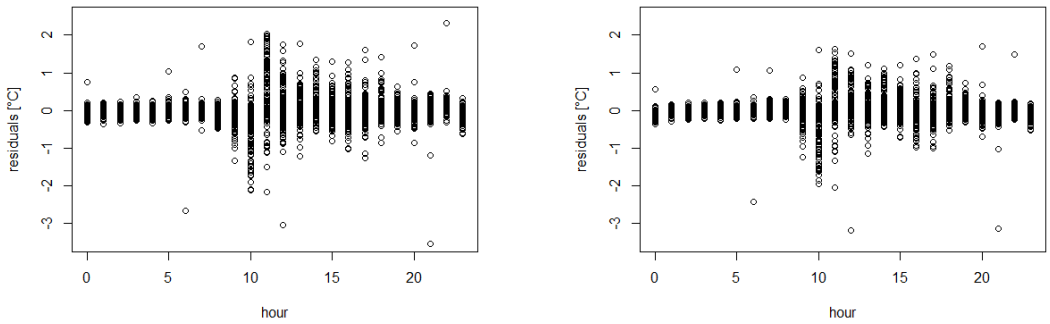

(a) Model eq. (2.1) **(b)** Model eq. (2.2)

Figure 15 – Residuals for the two models considered until now.

2.2.3 Solar Radiation Splines

From fig. 15 we see multiple issues, especially around 10 o'clock where we see an unexpected spike in temperatures. In this section we aim to include time-variable effective window area, since the angle where radiation hits the window changes. As suggested in task 2a we implement basis spline functions bs_k. Further, we try adding a radiation baseline γ:

$$
\begin{aligned}
dT_i &= \frac{1}{C_i}\left(\frac{1}{R_{ia}}(T_a - T_i) + \frac{1}{R_{im}}(T_m - T_i) + \Phi + p(G_v{+}\gamma)\sum_{k=1}^{5} a_k bs_k(t)\right)dt + \sigma_1 dw_1 \\
dT_m &= \frac{1}{C_m}\left(\frac{1}{R_{im}}(T_i - T_m) + R_{am}(T_a - T_m) + (1-p)(G_v{+}\gamma)\sum_{k=1}^{5} a_k bs_k(t)\right)dt + \sigma_2 dw_2 \\
yT_i &= T_i + \varepsilon
\end{aligned}
\tag{2.3}
$$

The five selected spline functions are plotted below:

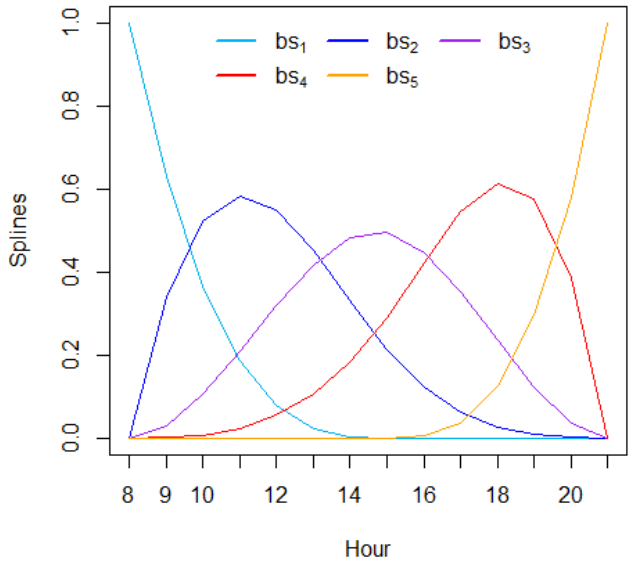

Figure 16 – The 5 splines indexed from left to right

The results of adding a variable window effect size plus enabling a potential constant light effect are shown below:

RSS	BIC
176.84	-68.133

Table 4 – Variable window effect & constant radiation results.

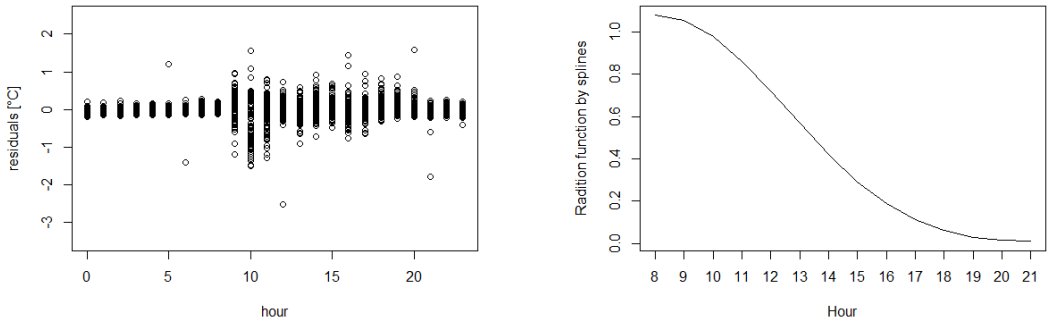

(a) Model eq. (2.3) **(b)** Time dependent sum of splines.

Figure 17 – Residuals and sum of splines from the CTSM optimization.

Although the floor is located in the east-most wing, we are surprised to obtain the spline function illustrated above. The current function implies that radiation plays a role even when the sun intensity is not peaking (early morning in the winter days). Fitting eq. (2.3) based on the known room temperatures, the new parameters are given by:

Coefficients	Estimate	Std. Error	t value	$\Pr(>\|t\|)$
a_1	$1.07\ 10^{0}$	$2.43\ 10^{-1}$	4.43	$9.59\ 10^{-6}$
a_2	$1.09\ 10^{0}$	$2.17\ 10^{-1}$	5.05	$4.73\ 10^{-7}$
a_3	$1.10\ 10^{-1}$	$9.80\ 10^{-2}$	1.13	$2.59\ 10^{-1}$
a_4	$1.01\ 10^{-2}$	$1.06\ 10^{-3}$	9.60	$0.00\ 10^{0}$
a_5	$1.02\ 10^{-2}$	$1.15\ 10^{-3}$	8.86	$0.00\ 10^{0}$
γ	$5.08\ 10^{0}$	$1.05\ 10^{0}$	4.85	$1.33\ 10^{-6}$
p	$9.95\ 10^{-1}$	$2.27\ 10^{-2}$	43.7	$0.00\ 10^{0}$

Table 5 – Estimates of selected coefficients including spline parameters and the minimum light threshold γ.

We keep all 5 splines, since all spline coefficients are significant in table 5. The estimated parameter reduces when the spline index increases as expected comparing fig. 16 and fig. 17. $\gamma = 5.08$ elucidate the importance of some constant radiation input for the current model.

Further, we note that suddenly $p = 0.96$ and it is therefore not significant to include anymore. Hence, with flexible window effect size the model assumes that the sun radiation only effects the indoor air and not the thermal mass. As we have not seen such behavior for p before, this is also an indication that the splines attempt to model more than just the sun radiation. Thus, instead of removing p as a parameter, we instead try adding other terms to our model with the aim of extracting actual sun radiation.

2.2.4 Neighbouring Rooms

Not being satisfied with our current tribute from the time dependent sum of splines, we try add another factor to our model. Specifically, we expect the maximum at 8 am to be caused by inertia in our system and not by solar radiation. To physically interpret such factors, we add temperature constraints from measurements from nearby rooms. We have for simplicity only looked at room 2 as it is directly connected with room 1. The combined model including the new neighbour constrained highlighted in red:

$$\begin{aligned} dT_i &= \frac{1}{C_i}\left(\frac{1}{R_{ia}}(T_a - T_i) + \frac{1}{R_{im}}(T_m - T_i) + \frac{1}{R_{i2}}(T_2 - T_i) + \Phi + p\zeta\right)dt + \sigma_1 dw_1 \\ dT_m &= \frac{1}{C_m}\left(\frac{1}{R_{im}}(T_i - T_m) + R_{am}(T_a - T_m) + (1-p)\zeta\right)dt + \sigma_2 dw_2 \\ yT_i &= T_i + \varepsilon \end{aligned} \tag{2.4}$$

where $\zeta = (G_v + \gamma)\sum_{k=1}^{5} a_k bs_k(t)$. Adding the influence of temperature in room 2 gives the following results:

RSS	BIC
129.87	-1084.115

Table 6 – Results adding impact from temperatures in neighbouring room.

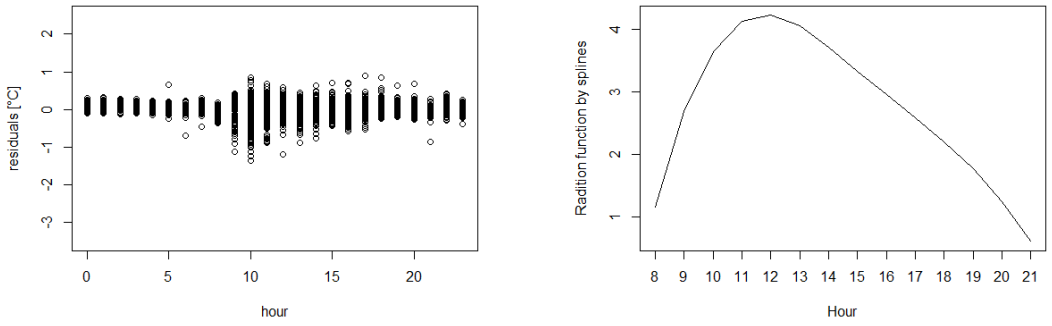

(a) Model eq. (2.4)

(b) Time dependent sum of splines.

Figure 18 – Residuals and sum of splines from the CTSM optimization.

We are pleased with the results from above. Notice that the sum of splines outputted from the CTSM optimization now defines a different function with peak around 12. With this new curve, the parameter p becomes significant again with a value close to 0.75. Thus, the model assume that 75% of the solar radiation hits the indoor air, while the rest directly impacts the thermal mass in room 1.

The residuals for each hour have approximately mean 0, many previous outliers have disappeared and finally the variances are generally reduced. Around 10 o'clock we still see some variance. We suspect human activities in the building (or lack of the same) to be the reason for these variations. A more detailed analysis on the topic of human activities is delivered through section 2.2.6. The inclusion of neighbouring rooms conclude the addition of direct physical parameters. Here we have reduced the RSS from initially 405 to 130.

2.2.5 Inertia From Heaters

Here we take back some steps as the temperate of neighboring rooms is not available at time t when we do multi-room forecasting. Therefore, we test some ideas without the neighbouring room as input. In fig. 12, we see that the heating power is switch off during the night and fluctuates a lot. We think that using the effect of heating directly might be incorrect as there might be some inertia we do not account for. Therefore, we introduce another state for the heaters:

$$\begin{aligned}
\mathrm{d}T_i &= \frac{1}{C_i}\left(\frac{1}{R_{ia}}(T_a - T_i) + \frac{1}{R_{im}}(T_m - T_i) + \frac{1}{R_{i\Phi}}(T_\Phi - T_i) + p\zeta\right)\mathrm{d}t + \sigma_1 \mathrm{d}w_1 \\
\mathrm{d}T_m &= \frac{1}{C_m}\left(\frac{1}{R_{im}}(T_i - T_m) + R_{am}(T_a - T_m) + (1-p)\zeta\right)\mathrm{d}t + \sigma_2 \mathrm{d}w_2 \\
\mathrm{d}T_\Phi &= \frac{1}{C_\Phi}\left(\frac{1}{R_{i\Phi}}(T_i - T_\Phi) + \Phi\right)\mathrm{d}t + \sigma_3 \mathrm{d}w_3 \\
yT_i &= T_i + \varepsilon
\end{aligned} \tag{2.5}$$

where $\zeta = (G_v + \gamma)\sum_{k=1}^{5} a_k bs_k(t)$.

RSS	BIC
164.83	-442.28

Table 7 – Results after adding the radiator as a state.

We see that this is not better than adding the inputs from neighbouring rooms, however, it is better than with the solar splines only (section 2.2.3).

2.2.6 Human Activity

Until now, we have primarily discussed potential direct measurable physical inputs to the model. However, these buildings are used by peoples at the university hence we speculated that they could have an impact on the indoor temperature. In fig. 13, we saw that the temperature is lower in the weekends where we would also expect fewer people in the rooms. In figure 12, we saw that there seems to be some weeks around end of 2014 and a week in 2015 where yTi_1 dropped. As universities are often closed on public holidays, we suspected that this could be the case here. On an hourly basis, we see in fig. 13 that there seems to be some peak hours around 8-16 which could also be the standard opening hours. Therefore, we introduce the indicator variables $\mathbf{1}_{not\,holiday}$, $\mathbf{1}_{weekday}$ and $\mathbf{1}_{peak\,hour}$. Let $d_i \in [1, 2, .., 7] \in \mathbb{Z}^7$ denote the day of the week for the ith observation and let $h_i \in [1, 2, .., 24] \in \mathbb{Z}^{24}$ denote the hour of the ith observation. Then we introduce indicator variables

$$\begin{aligned}
\mathbf{1}_{weekday} &= \begin{cases} 1 & \text{if } d_i \in [1, 2, ..., 5] \\ 0 & \text{otherwise} \end{cases} \\
\mathbf{1}_{peak\,hour} &= \begin{cases} 1 & \text{if } h_i \in [8, 9, ..., 16] \\ 0 & \text{otherwise} \end{cases}
\end{aligned} \tag{2.6}$$

For the holidays, we used online resources [3] [4] to encode the public and regional holidays. On the basis of that, we made an indicator variable $\mathbf{1}_{not\,holiday}$.

We can now define the indicator variable for peak hours during a normal business week as

$$\mathbf{1}_{weekly\,peaks} = \mathbf{1}_{not\,holiday}\mathbf{1}_{weekday}\mathbf{1}_{peak\,hour} \tag{2.7}$$

In our modelling, we tried many things with this variable; added it to the noise term, directly to the ambient temperature and in the radiator state equation. The best results where obtain in the two latter cases with where we added a term $c_{weekly\,peaks}\mathbf{1}_{weekly\,peaks}$ s.t. for the case where we added it to the radiator equation:

$$\begin{aligned}
\mathrm{d}T_i &= \frac{1}{C_i}\left(\frac{1}{R_{ia}}(T_a - T_i) + \frac{1}{R_{im}}(T_m - T_i) + \frac{1}{R_{i\Phi}}(T_\Phi - T_i) + p\zeta\right)\mathrm{d}t + \sigma_1\mathrm{d}w_1 \\
\mathrm{d}T_m &= \frac{1}{C_m}\left(\frac{1}{R_{im}}(T_i - T_m) + \frac{1}{R_{am}}(T_a - T_m) + (1-p)\zeta\right)\mathrm{d}t + \sigma_2\mathrm{d}w_2 \\
\mathrm{d}T_\Phi &= \frac{1}{C_\Phi}\left(\frac{1}{R_{i\Phi}}(T_i - T_\Phi) + c_{weekly\,peaks}\mathbf{1}_{weekly\,peaks} + \Phi\right)\mathrm{d}t + \sigma_3\mathrm{d}w_3 \\
yT_i &= T_i + \varepsilon
\end{aligned} \tag{2.8}$$

here we remove some of the splines as they turned out to be insignificant s.t. $\zeta = (G_v + \gamma)\left(a_1 bs_1(t) + a_3 bs_3(t)\right)$

	RSS	BIC
Humans affects ambient air	154.03	-646.80
Humans affects radiator	149.08	-772.35

Table 8 – Results after adding human affects

Including human activity in the radiator equation seems to work best. The argument for modelling the system in that way is that human presence will increase the temperature in the room.

2.2.7 Evaluation and discussion of models

In the section above, we notice that the models where we use the neighbouring room as inputs have the best performance. We suspect this is because some of the variability from unknown factors could be partly captured in the temperature dynamics of the second room and subsequently taken into account in our model for the first room. Together with adding the neighbouring room we have also increased the complexity of both thermal mass and solar radiation. Individually they add information to the temperature, as the equations become more aligned with some of the real physical conditions. This enable a better classification of initial 'hidden' parameters such as room heat inertia which seems highly relevant. Below, we mention some of the restrictions / limits with our current model:

We have some parameters such as γ and p that are highly varying with respect to small changes. Although they are (nearly always) noted as significant for our models, they clearly cover more than their given physical interpretation. This is clear when we try include peak hours to model the added heat that arises from human activity and multiple spline turn out insignificant. In general the highest values achieved for the global solar radiation, G_v, are around 0.8 while γ often attain values around 5. As $G_v << \gamma$, we speculate that some of the affect of human present in the room is captured in γ because the splines for solar radiation is only defined in the same hours where humans would also be present.

We have tried to change the variance term of our systems and make them varying dependent on input parameter. In general, this has decreased the predictability and hence were not included. To further lower the residuals at the critical time 10 o'clock such extensions should be considered. Although our current best model improves at 10 o' clock as well, it is still the time with highest residuals.

Finally, to evaluate our final best model 'including neighbouring room' with RSS 130 we first check for stability: After 4 iterations with the optimal found parameters, the optimization returns with the same RSS and approximately the same parameter. Further when perturbating a single parameter (for example p by 0.1) we again obtain 130 as our RSS after around 30 iterations. Thus, our solution is locally stable which is very important when identifying it.

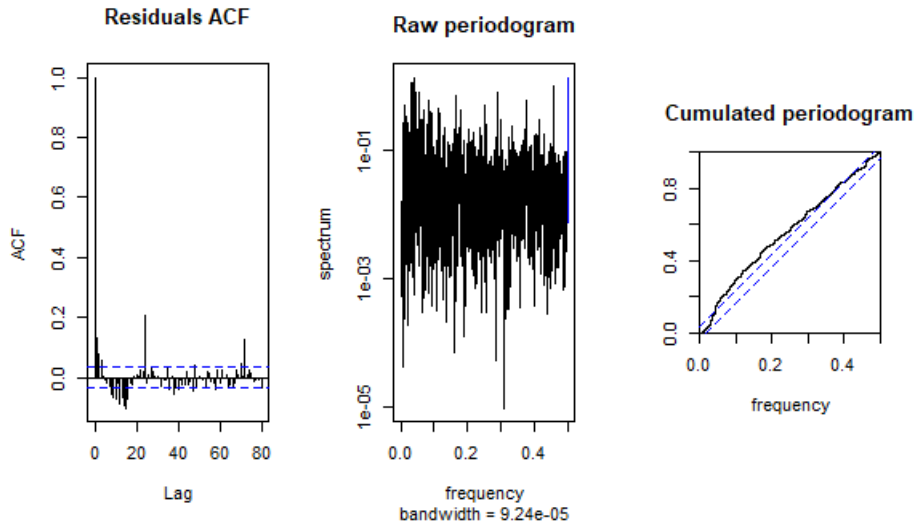

Figure 19 – Residual analysis for the neighbouring room model of eq. (2.4).

In figure 19, we see a dramatic improvement in the residuals compared to the baseline in figure 14. There is still some variation the model cannot capture which we see in as the systematic oscillations in the ACF. The cumulated periodogram also suggest that the errors do not pass the white noise test though we have a couple of frequencies with well defined steps. We conclude that there is still some systematic variance, that we cannot capture in our model, however, residuals of the final model are more white than for baseline.

2.2.8 Further Recommended Extensions

In this short section we will briefly mention some ideas to extending our single room model with the hope of constituting a stimulus for research in such directions:

Consider a t dependent parameter
Having seen from fig. 11 that time t is actually more correlated with $yTi1$ than the ambient temperature T_a, it should be considered to include t in our models. There are multiple solutions taking t into account - it could be:

- a variable classifying the current season and month of each data point.

- an underlying seasonal trend function found in data.

Both methods might add to the understanding of building inertia. Initial results have shown that, when including neighbouring room, advanced heating or human activities the additional information from t is limited.

Delayed differential equations
To improve the models, one could consider using lagged values of the temperature measurements and define a systems using delay differential equations. This could potentially better capture seasonality in the data.

Time series features
To better describe the characteristics of the propagating process, one could consider using features s.t. the max or min temperatures from the day before, mean of the last week or latest two days. This could potentially also better capture more of the inertia of the system and better characterise the system.

2.3 Part 3b: Making a Multi-room Model

In the following, we will use the floor plan of fig. 10 and the indicated room numbers. We focus first on coupling the northern part of the building i.e. room 1, 2 and then expand to the southern.

2.3.1 Northern part of the building

We first assume that the thermal mass for room 1 and 2 can be modeled as a single state and there is a direct transfer of the indoor temperatures of the two rooms

$$
\begin{aligned}
\mathrm{d}T_1 &= \frac{1}{C_1}\left[\frac{1}{R_{1a}}\left(T_a - T_1\right) + \frac{1}{R_{1m}}\left(T_m - T_1\right) + \frac{1}{R_{1\Phi}}\left(T_\Phi - T_1\right) + \frac{1}{R_{12}}\left(T_2 - T_1\right) + p\zeta\right]\mathrm{d}t + \sigma_1 \mathrm{d}w_1 \\
\mathrm{d}T_2 &= \frac{1}{C_2}\left[\frac{1}{R_{2a}}\left(T_a - T_2\right) + \frac{1}{R_{2m}}\left(T_m - T_2\right) + \frac{1}{R_{2\Phi}}\left(T_\Phi - T_2\right) + \frac{1}{R_{12}}\left(T_1 - T_2\right)\right]\mathrm{d}t + \sigma_2 \mathrm{d}w_2 \\
\mathrm{d}T_\Phi &= \frac{1}{C_\Phi}\left(\frac{1}{R_{i\Phi}}\left(T_1 - T_\Phi\right) + \frac{1}{R_{i\Phi}}\left(T_2 - T_\Phi\right) + c_{weekly\ peaks}\mathbf{1}_{weekly\ peaks} + \Phi\right)\mathrm{d}t + \sigma_3 \mathrm{d}w_3 \\
\mathrm{d}T_m &= \frac{1}{c_m}\left[\sum_{i=1}^{2}\frac{1}{R_{im}}\left(T_i - T_m\right)\right]\mathrm{d}t + \sigma_3 \mathrm{d}w_4 \\
yT_1 &= T_1 + \varepsilon \\
yT_2 &= T_2 + \varepsilon
\end{aligned}
\tag{2.9}
$$

With the model specified in 2.9 we obtained the following RSS values for the rooms:

Rooms	RSS
Room 1	176.83
Room 2	48.41
Total	225.24

Table 9 – Results for model of eq. (2.9).

If we compare the results of room 1 with what we obtained in the previous models, then we see that the RSS is not as good. However, these results can be serve as a baseline model to be compared with the system where we couple all rooms. Therefore, we use the same model for the southern part:

2.3.2 Southern part of the building

If we setup the exact same system of equation 2.9 for the southern part, i.e. room 3 and 4, then we get the results shown in table 10 shown on the top of the next page. The results suggests that room 1 is definitely the hardest to model, while the three other rooms obtain similar RSS values.

Rooms	RSS
Room 3	51.17
Room 4	55.06
Total	106.23

Table 10 – Results for model of table 10.

2.3.3 Modelling the Whole Building

Having looked at separate parts of the second floor of the east-most wing, we now aim to model the entire area. Thus our model must estimate the indoor temperature of all 4 rooms, where a temperature sensor is located.

2.3.4 Baseline Model

We first try to model the 4 rooms by assuming a state for every rooms air temperature while only having a single thermal mass state. The choice of only including 5 states in our initial baseline model is for numerical reasons. Thus, we assume a design like:

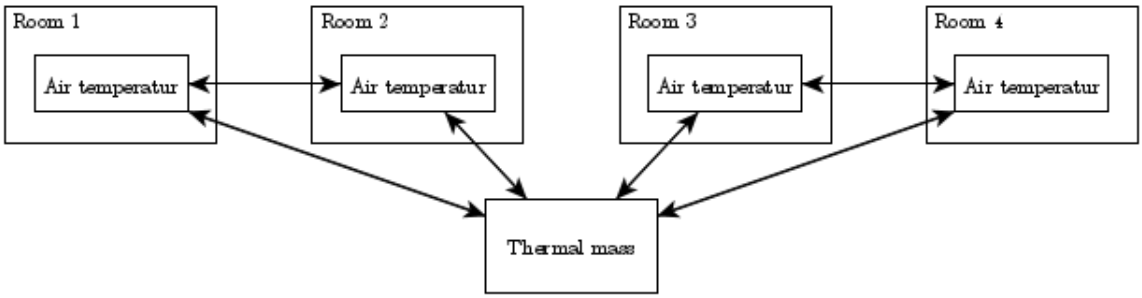

Figure 20 – Multiroom baseline model with only one thermal mass.

Here we predict that the air temperature of northern and southern part should not be directly connected. The assumption is solely based on fig. 10 where we see a clear separation between room 1 & 2 and room 3 & 4. Besides the increased complexity using the design from fig. 20, the multi-room baseline model is designed similarly to the one for a single:

$$
\begin{aligned}
dT_1 &= \frac{1}{C_1}\left(\frac{1}{R_{1a}}(T_a - T_1) + \frac{1}{R_{1m}}(T_m - T_1) + \frac{1}{R_{12}}(T_2 - T_1) + \Phi_N + A_w G_v\right)dt + \sigma_1 dw_1 \\
dT_2 &= \frac{1}{C_2}\left(\frac{1}{R_{2a}}(T_a - T_2) + \frac{1}{R_{2m}}(T_m - T_2) + \frac{1}{R_{12}}(T_1 - T_2) + \Phi_N\right)dt + \sigma_2 dw_2 \\
dT_3 &= \frac{1}{C_3}\left(\frac{1}{R_{3a}}(T_a - T_3) + \frac{1}{R_{3m}}(T_m - T_3) + \frac{1}{R_{34}}(T_4 - T_3) + \Phi_S\right)dt + \sigma_3 dw_3 \\
dT_4 &= \frac{1}{C_4}\left(\frac{1}{R_{4a}}(T_a - T_4) + \frac{1}{R_{4m}}(T_m - T_4) + \frac{1}{R_{34}}(T_3 - T_4) + \Phi_S + A_w G_v\right)dt + \sigma_4 dw_4 \\
dT_m &= \frac{1}{C_m}\left(\frac{1}{R_{1m}}(T_1 - T_m) + \frac{1}{R_{2m}}(T_2 - T_m) + \frac{1}{R_{3m}}(T_2 - T_3) + \frac{1}{R_{4m}}(T_4 - T_m)\right)dt + \sigma_5 dw_5 \\
yT_i &= T_i + \varepsilon \text{ for } i \in 1, \ldots, 4
\end{aligned}
\tag{2.10}
$$

Here Φ_N and Φ_S respectively denote the north and south heating system. Comparing our estimated yTi for $i \in 1, \ldots, 4$ based on eq. (2.10) we obtain these residual sum of squares:

Rooms	RSS
Room 1	247.3
Room 2	77.81
Room 3	71.07
Room 4	56.92
Total	453.1

Table 11 – Results for model of 2.10

The residuals through a day are plotted on the next page. For room 1 we see patterns similar to the results from the single room baseline model although the RSS value is lower.

2.3.5 Solar Radiation

The single-room results suggest, that a potential issue with our multi-room baseline model is the way we model solar radiation. We only add the impact of solar radiation directly in the equations for room 1 and 4 and we add the same amount for both rooms independent on their location and time of the day. For numerical reasons we still restrict our self to only look at solar radiation in the expected most sensitive rooms: room 1 and 4, but now we add independent splines for both. We obtain:

$$
\begin{aligned}
dT_1 &= \frac{1}{C_1}\left(\frac{1}{R_{1a}}(T_a - T_1) + \frac{1}{R_{1m}}(T_m - T_1) + \frac{1}{R_{12}}(T_2 - T_1) + \Phi_N + \zeta_1\right)dt + \sigma_1 dw_1 \\
dT_2 &= \frac{1}{C_2}\left(\frac{1}{R_{2a}}(T_a - T_2) + \frac{1}{R_{2m}}(T_m - T_2) + \frac{1}{R_{12}}(T_1 - T_2) + \Phi_N\right)dt + \sigma_2 dw_2 \\
dT_3 &= \frac{1}{C_3}\left(\frac{1}{R_{3a}}(T_a - T_3) + \frac{1}{R_{3m}}(T_m - T_3) + \frac{1}{R_{34}}(T_4 - T_3) + \Phi_S\right)dt + \sigma_3 dw_3 \\
dT_4 &= \frac{1}{C_4}\left(\frac{1}{R_{4a}}(T_a - T_4) + \frac{1}{R_{4m}}(T_m - T_4) + \frac{1}{R_{34}}(T_3 - T_4) + \Phi_S + \zeta_4\right)dt + \sigma_4 dw_4 \\
dT_m &= \frac{1}{C_m}\left(\frac{1}{R_{1m}}(T_1 - T_m) + \frac{1}{R_{2m}}(T_2 - T_m) + \frac{1}{R_{3m}}(T_2 - T_3) + \frac{1}{R_{4m}}(T_4 - T_m)\right)dt + \sigma_5 dw_5 \\
yT_i &= T_i + \varepsilon \text{ for } i \in 1, \ldots, 4
\end{aligned}
\tag{2.11}
$$

where $\zeta_1 = (G_v + \gamma)\sum_{k=1}^{5} a_k bs_k(t)$ and $\zeta_4 = (G_v + \gamma)\sum_{k=1}^{5} b_k bs_k(t)$.

The model takes about 4 hours to fit on a standard laptop and we achieve the residual sum of squares given in table 12.

Rooms	RSS
Room 1	203.77
Room 2	69.38
Room 3	57.13
Room 4	56.07
Total	386.4

Table 12 – Results for model of 2.11

We see that room 1, 2, and 3 is improved over the baseline model but room 4 has almost exactly the same RSS. This has maybe something to do with that room 4 is north facing and hence the sun will not affect this facade much in the winter time.

2.3.6 Extended Structure

Lastly we try to model the 4 rooms by assuming a state for every rooms air temperature and thermal mass. We model their interaction by assuming every rooms thermal mass and air temperature can interact neighbouring rooms except for the air temperature of room 2 and 3 because these are not directly connected. The model is illustrated in figure 21

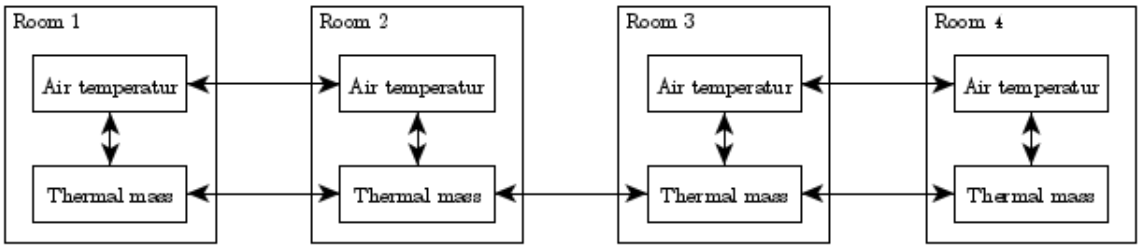

Figure 21 – Multiroom with multiple different thermal masses.

We further assume that the radiators affect air temperature, solar radiation affects both air temperature and thermal mass and ambient temperature also affects air temperature and thermal mass. This gives the equations

$$
\begin{aligned}
\mathrm{d}T_1 &= \frac{1}{C_1}\left(\frac{1}{R_{1a}}(T_a - T_1) + \frac{1}{R_{1m_1}}(T_{m_1} - T_1) + \frac{1}{R_{12}}(T_2 - T_1) + \Phi_N + p_1\zeta_1\right)\mathrm{d}t + \sigma_1\mathrm{d}w_1 \\
\mathrm{d}T_{m_1} &= \frac{1}{C_{m_1}}\left(\frac{1}{R_{1m_1}}(T_1 - T_{m_1}) + \frac{1}{R_{am_1}}(T_a - T_{m_1}) + \frac{1}{R_{m_1m_2}}(T_{m_1} - T_{m_2}) + (1-p_1)\zeta_1\right)\mathrm{d}t + \sigma_2\mathrm{d}w_2 \\
\mathrm{d}T_2 &= \frac{1}{C_2}\left(\frac{1}{R_{2a}}(T_a - T_2) + \frac{1}{R_{2m_2}}(T_{m_2} - T_2) + \frac{1}{R_{12}}(T_1 - T_2) + \Phi_N + p_2\zeta_2\right)\mathrm{d}t + \sigma_3\mathrm{d}w_3 \\
\mathrm{d}T_{m_2} &= \frac{1}{C_{m_2}}\Big(\frac{1}{R_{2m_2}}(T_2 - T_{m_2}) + \frac{1}{R_{am_2}}(T_a - T_{m_2}) + \frac{1}{R_{m_1m_2}}(T_{m_2} - T_{m_1}) + \frac{1}{R_{m_2m_3}}(T_{m_2} - T_{m_3}) \\
&\quad + (1-p_2)\zeta_2\Big)\mathrm{d}t + \sigma_4\mathrm{d}w_4 \\
\mathrm{d}T_3 &= \frac{1}{C_3}\left(\frac{1}{R_{3a}}(T_a - T_3) + \frac{1}{R_{3m_3}}(T_{m_3} - T_3) + \frac{1}{R_{43}}(T_4 - T_3) + \Phi_S + p_3\zeta_3\right)\mathrm{d}t + \sigma_5\mathrm{d}w_5 \\
\mathrm{d}T_{m_3} &= \frac{1}{C_{m_3}}\Big(\frac{1}{R_{3m_3}}(T_3 - T_{m_3}) + \frac{1}{R_{am_3}}(T_a - T_{m_3}) + \frac{1}{R_{m_4m_3}}(T_{m_3} - T_{m_4}) + \frac{1}{R_{m_2m_3}}(T_{m_3} - T_{m_2}) \\
&\quad + (1-p_3)\zeta_3\Big)\mathrm{d}t + \sigma_6\mathrm{d}w_6 \\
\mathrm{d}T_4 &= \frac{1}{C_4}\left(\frac{1}{R_{4a}}(T_a - T_4) + \frac{1}{R_{4m_4}}(T_{m_4} - T_4) + \frac{1}{R_{43}}(T_3 - T_4) + \Phi_S + p_4\zeta_4\right)\mathrm{d}t + \sigma_7\mathrm{d}w_7 \\
\mathrm{d}T_{m_4} &= \frac{1}{C_{m_4}}\left(\frac{1}{R_{4m_4}}(T_4 - T_{m_4}) + \frac{1}{R_{am_4}}(T_a - T_{m_4}) + \frac{1}{R_{m_4m_3}}(T_{m_4} - T_{m_3}) + (1-p_4)\zeta_4\right)\mathrm{d}t + \sigma_8\mathrm{d}w_8 \\
yT_i &= T_i + \varepsilon \text{ for } i \in 1, \ldots, 4
\end{aligned}
\tag{2.12}
$$

The model is now very large and on a standard laptop it took 84 hours to fit. Hence it is certainly not practical to use this many states and parameters. In table 13 the residual sum of squares is stated.

Rooms	RSS
Room 1	190.59
Room 2	56.29
Room 3	47.61
Room 4	42.96
Total	337.45

Table 13 – Results for model of 2.12

We see we get an improvement of approximately 10 in RSS for each room compared to the model 2.11. In percentage we achieve an improvement of 12.5% which is an okay improvement but it also comes with a huge increase in model complexity and the fitting time increases with over 2000%.

3 References

[1] U. Høgsbro Thygesen, *Diffusion and Stochastic Differential Equations*. DTU Compute, 2021.

[2] Sdetools. [Online]. Available: https://github.com/Uffe-H-Thygesen/SDEtools/tree/master/R

[3] Holidays and observances in spain in 2014. [Online]. Available: https://www.timeanddate.com/holidays/spain/2014

[4] Public holidays in spain in 2015. [Online]. Available: https://www.officeholidays.com/countries/spain/2015